ISA Transactions 97 (2020) 1–13

Contents lists available at ScienceDirect

ISA Transactions

journal homepage: www.elsevier.com/locate/isatrans

Research article

Improved integral backstepping control of variable speed motion systems with application to a laboratory helicopter

A. Haruna [a,b], Z. Mohamed [a,*], M.Ö. Efe [c], M.A.M. Basri [a]

[a] School of Electrical Engineering, Universiti Teknologi Malaysia, 81310 UTM, Johor Bahru, Johor, Malaysia
[b] Department of Mechatronics Engineering Bayero University Kano, Nigeria
[c] Department of Computer Engineering, Hacettepe University, Turkey

HIGHLIGHTS

- We propose an improved integral backstepping control for a laboratory helicopter.
- The method can simultaneously handle constant and time varying input references.
- A switched backstepping control is designed to reduce the effects of noise and jerking.
- Experiments show better transient response and tracking performance.
- The method is also robust to external wind disturbance.

ARTICLE INFO

Article history:
Received 12 February 2018
Received in revised form 4 May 2019
Accepted 8 July 2019
Available online 10 July 2019

Keywords:
Backstepping
Conditional integral
Regulation
MIMO
Switching
Noise
TRAS/TRMS

ABSTRACT

This paper proposes an improved method of integral backstepping for real time control of a laboratory helicopter with variable speed rotors known as the Two-Rotor Aero-dynamic System (TRAS). The coupled system is decomposed into the horizontal subsystem (HS) and the vertical subsystem (VS) and traditional backstepping, augmented with direct integral action is designed for each subsystem. The transient response to both constant and time varying references is then simultaneously improved by modifying an already proposed method called dual boundary conditional integration. A switching technique is also employed to enhance the tracking response of the undamped HS for its bi-directional motor which exhibits jerking effects. Experimental results show that the proposed approach yields improved transient and tracking performance when compared to previously proposed methods exploiting conditional integration earlier proposed for improving the transient response of controlled nonlinear systems with integral action. The results also show the robustness of the proposed method in the presence of the coupling effects and additional external disturbance applied to the system in the form of a wind gust.

1. Introduction

The Two Rotor Aero-dynamical System (TRAS) exemplifies a highly nonlinear system with significant cross couplings and unmeasurable states and is regarded as a challenging control problem. The helicopter-like system consists primarily of main and tail rotors attached to the ends of a beam. The control objective is to track a predetermined trajectory quickly and accurately by controlling the thrusts generated from the system's variable speed rotors.

Many motion control systems like the TRAS can be represented as a cascade of systems from the input to output. These systems can thus be represented in triangular form or in strict-feedback form when the component subsystems are nonlinear. Over the years, recursive backstepping has proven to be an effective approach in designing nonlinear control laws for this class of systems. Robust output regulation, which is one of the most essential problems in control engineering practice [1,2], can then be achieved by introducing integral action into the controller. This is especially required in the presence of parameter uncertainties and/or constant external disturbances. Integral action, however, has the well-known drawback of degrading the transient performance by instigating undesirable overshoot and oscillations which can lead to longer settling times or even instability.

The most widely used method of including integral action in backstepping, which is a natural choice for controlling cascaded nonlinear systems, is to use parameter adaptation [3,4]. However, parameter adaptation has the drawback of degrading the transient performance when initiated [5]. Several methods including multiple models [6], neural networks [7] and estimator resetting [8] for example, have been employed to reduce

* Corresponding author.
E-mail address: zahar@fke.utm.my (Z. Mohamed).

https://doi.org/10.1016/j.isatra.2019.07.016
0019-0578/

this drawback. In addition to degrading transient performance, parameter update laws also significantly complicate the computation of the control signal. A relatively straight-forward approach introduced in [9] includes direct integral action by augmenting the first step of the backstepping design with an integral of the output error. While this method also degrades the transient performance, it can be improved by manipulating the gain parameter of the integrator.

In feedback controllers with direct integral action, methods like integrator resetting [10–12] have been proposed to improve the transient response. In [13] and [14], a variable gain integral controller was proposed to solve this problem in linear plants. For nonlinear systems, the concept of conditional integration (providing integral action conditionally within a specific boundary) was introduced in [15] in a Sliding Mode Control (SMC) framework. This was extended using Lyapunov redesign to a general class of state feedback controllers in [16]. More recently, an improved method of conditional integration, which uses dual boundaries, has been developed in [17]. The proposed method was validated by simulation on a Two Rotor MIMO System (TRMS), a variant of the TRAS with different physical parameters. While this method showed improvement in the transient response, only simulation results were provided and an integral reset was required for sinusoidal reference signals. Moreover, the method in [17] cannot simultaneously handle constant and time-varying references.

Another problem commonly encountered in practice is the measurement noise emanating from used sensory devices. This is especially the case when state dependent feedback laws (like backstepping), which require system states for computation of the control law, are employed. The problem is further complicated when not all required states are available for measurement (as is often the case) and have to be observed or estimated. Although the tracking performance might not be seriously affected by the measurement noise [18,19], noise in the observed quantities leads to saturation of the actuators, vibrations and decreased motor efficiency [20]. While saturation of the control input may be applied to mitigate the jerking effects in variable speed motors, this cannot be applied when bi-directional rotation of the motor is required, and the motor current has to be reversed.

In the literature, many practical control approaches have been proposed for the TRAS/TRMS. PID based controllers have been implemented in [21,22]. These, however, have narrow operating ranges and do not yield a fast and satisfactory performance as the system's inextricably intertwined nonlinearities are not specifically taken into consideration. PID based Active Disturbance Rejection Control (ADRC) was proposed for the TRAS in [23] in which only tracking of step-wise constant waveforms was investigated. More recently, ADRC has also been proposed for the TRMS in [24] in combination with an input shaper to improve the transient performance and in [25] using a cascaded structure. The non-cascaded ADRC schemes for the TRAS/TRMS in [23] and [24] showed good tracking of step-wise constant input signals, but the tracking of time varying input waveforms was not investigated. Although the proposed cascaded ADRC structure in [25] showed good tracking of slowly time varying references for the VS, the tracking response of the HS and the transient responses of both subsystems could be improved. Fractional order PID has also been suggested for the TRMS in [26] but the results obtained to a step input showed significant overshoot and oscillation in the transient phase.

Nonlinear methods like feedback linearisation [27,28], SMC [29–34], and backstepping [35,36] have also been suggested for practical control implementation on the TRAS/TRMS and showed satisfactory tracking and robustness, especially for the HS. The feedback linearisation method in [27] for the TRMS was designed using a 2-step approach to improve the working range, while that in [28] was implemented using second level adaptation to enhance performance. The terminal SMC [29] and the integral SMC [30] proposed for the TRMS achieved tracking but showed quite long settling times while the integral SMC [31] for the TRAS was only subjected to ramp like changes in the reference. The effects of chattering with SMC were considerably attenuated by employing a sliding mode differentiator on the TRAS in [32] and a fuzzy compensator on the TRMS in [33]. The proposed SMC for the TRAS in [34] used a model-free approach to tune the parameters but the system displayed significant tracking error for a sinusoidal signal. The backstepping controller proposed for the TRMS in [35] employed an intelligent observer to provide estimates of inaccessible states while that for the TRAS in [36] used a disturbance observer to improve robustness.

In general, the nonlinear methods proposed for the TRAS/TRMS showed relatively satisfactory tracking and robustness, especially for the yaw angle. However, with the exception of [28] where multiple models were employed, none of the aforementioned works directly address the issue of improving the transient performance or alleviating the jerking effects in the rotors in real time. Moreover, the experimental results for the TRMS in [28] showed significant overshoots and tracking error, especially for the pitch angle. Thus, the contribution of this paper to address these issues is twofold. First, the method of Dual Boundary Conditional Integration (DBCI) in [17] which varies the integral gain parameter to improve transient and tracking performance is enhanced. As opposed to being a function of the reference signal, the sign of the incremental variable integral gain of the DBCI law [17] during the transient phase is modified such that it is dependent on the sign of the error state. This allows the modified DBCI (MDBCI) law proposed in this work to simultaneously handle both constant and time varying input references and moreover, eliminates the need for integral resetting. Second, the MDBCI law is combined with a switched control method between two candidate integral backstepping controllers to reduce jerking in the bi-directional tail rotor of the HS and improve the overall performance of the coupled system. In addition, real time experimental validation of the proposed approach is achieved in the presence of model uncertainties, measurement noise and wind gusts.

The rest of this paper is organised as follows. Section 2 describes the mathematical model of the TRAS, Section 3 presents the integral backstepping control design and Section 4 presents the proposed approach that improves the transient response and tracking performance. Stability of the closed-loop system under the proposed control method is analysed in Section 5, experimental results are presented and discussed in Section 6 and concluding remarks are given in Section 7.

2. Dynamic model of the TRAS

The TRAS shown in Fig. 1 consists of a free beam pivoted at its base. The articulated joint enables the beam to rotate such that its ends move on the horizontal (yaw) and vertical (pitch) planes. The main and tail rotors are driven by 12 V DC motors and are attached to the ends of the beam. A counterbalance arm with a weight at its end is fixed to the beam at the pivot to provide damping. The system is balanced in such that the main rotor side of the beam is lowered when the motors are switched off.

Unlike conventional helicopters where aerodynamic thrust is produced by altering the angle of attack of each propeller, aerodynamic thrust in the TRAS is generated by increasing the rotation speed of the rotors. The rotor speeds (measured by tachogenerators) and the pitch and yaw angles (measured by digital position encoders) are the four controlled variables to be controlled by manipulating the main and tail rotor torques. An approximate

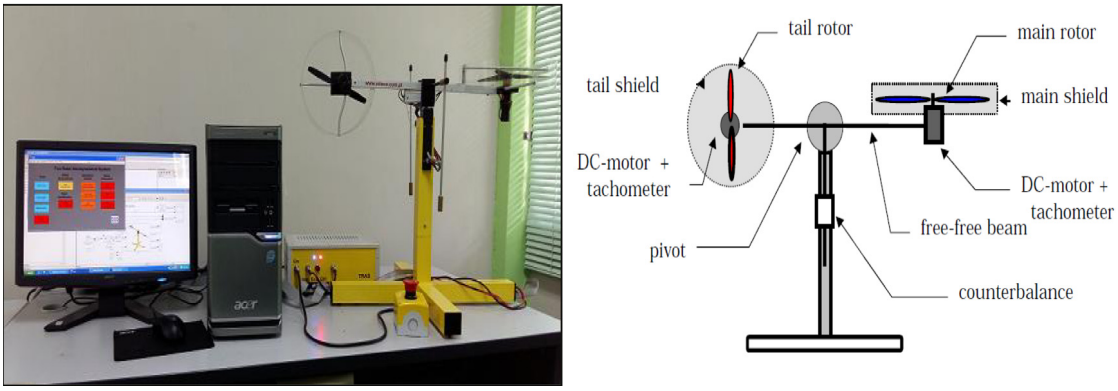

Fig. 1. (a) TRAS experimental setup, (b) TRAS component parts.

mathematical model of the TRAS is obtained by using Newton's second law of motion and converted into state-space form [37]. The equations defining the motion of the TRAS are given in (1) with values of the physical parameters provided in Table 1. For the rest of this article, subscripts h and v respectively, will be used to represent the horizontal and vertical subsystems of the TRAS.

$$\begin{aligned}
\dot{x}_1 &= x_3 \\
\dot{x}_2 &= x_4 \\
\dot{x}_3 &= \frac{1}{J_h}\left[l_t F_h(x_5)\cos x_2 - k_h x_3 + u_v k_{vh} - a_1 x_3 |x_5|\right] \\
\dot{x}_4 &= \frac{1}{J_v}\Big[l_m F_v(x_6) - k_v x_4 + g\left((A-B)\cos x_2 - C\sin x_2\right) \\
&\quad -\frac{1}{2}x_3^2 (A+B+C)\sin(2x_2) u_h k_{hv} + u_h k_{hv} - a_2 x_4 |x_6|\Big] \\
\dot{x}_5 &= \frac{1}{I_h}\left(u_h - H_h^{-1}(x_5)\right) \\
\dot{x}_6 &= \frac{1}{I_v}\left(u_v - H_v^{-1}(x_6)\right).
\end{aligned} \tag{1}$$

where x_1 (x_2) is the yaw (pitch) angle of the beam, x_3 (x_4) is the angular velocity of the beam around the horizontal (vertical) axis, u_h (u_v) is the input voltage to the tail (main) rotor, x_5 (x_6) is the tail (main) rotor speed and F_h (F_v) is the propulsive force it generates, and H_h (H_v) is a dynamical equation of the tail (main) rotor.

The sum of the moments of inertia relative to the vertical axis J_h depends on the position, x_2 of the beam and can be expressed as:

$$J_h = D\sin^2 x_2 + E\cos^2 x_2 + F. \tag{2}$$

The nonlinear relationships between the motor input voltages, rotor speeds and the aerodynamic thrusts generated (static characteristics) are determined experimentally for each device [37] and approximated by the polynomials in (3)–(6).

$$\begin{aligned}
\omega_h \approx &-2.2\times10^3 {u_h}^5 - 1.7\times10^2 {u_h}^4 - 4.5\times10^3 {u_h}^3 \\
&+ 3\times10^2 {u_h}^2 \\
&+ 9.8\times10^3 u_h - 9.2,
\end{aligned} \tag{3}$$

$$\begin{aligned}
F_h \approx &-2.6\times10^{-20}{\omega_h}^5 + 4.1\times10^{-17}{\omega_h}^4 + 3.2\times10^{-12}{\omega_h}^3 \\
&- 7.3\times10^{-9}{\omega_h}^2 \\
&+ 2.1\times10^{-5}\omega_h + 0.0091,
\end{aligned} \tag{4}$$

$$\begin{aligned}
\omega_v \approx &-5.2\times10^3 {u_v}^7 - 1.1\times10^2 {u_v}^6 + 1.1\times10^4 {u_v}^5 \\
&+ 1.3\times10^2 {u_v}^4 \\
&- 9.2\times10^3 {u_v}^3 - 31{u_v}^2 + 6.1\times10^3 u_v - 4.5,
\end{aligned} \tag{5}$$

$$\begin{aligned}
F_v \approx &-1.8\times10^{-18}{\omega_v}^5 - 7.8\times10^{-16}{\omega_v}^4 + 4.1\times10^{-11}{\omega_v}^3 \\
&+ 2.7\times10^{-8}{\omega_v}^2 \\
&+ 3.5\times10^{-5}\omega_v - 0.014.
\end{aligned} \tag{6}$$

Remark 1. The model in (1) represents coupled dynamics, where the behaviour of HS and VS influence each other in such a way that the scheduling of a proper control signal meeting the stability and performance expectations is challenging. Also, the model is derived under a set of assumptions and simplifications regarding delays, rigidity issues and the like and obtaining precision with speed is a design challenge attacked by many researchers.

3. Integral backstepping control design

The integral backstepping controller (IBC) is individually designed using traditional recursive backstepping procedure [38,39] for the decomposed HS and VS by taking the cross coupling effects as uncertainties. The integral of the error is added to the first step of the backstepping design [9,40] to provide robustness against the coupling and modelling uncertainties.

3.1. Horizontal subsystem integral backstepping

The decomposed model of the HS can be obtained as [37]

$$\begin{aligned}
\dot{x}_1 &= x_3 \\
\dot{x}_3 &= \frac{1}{J_h}\left[l_t F_h(x_5)\cos x_2 - k_h x_3 - a_1 x_3 |x_5|\right] \\
\dot{x}_5 &= \frac{1}{I_h}\left(u_h - H_h^{-1}(x_5)\right).
\end{aligned} \tag{7}$$

Let:

$$z_1 := x_1 - x_{1d}, \tag{8}$$

$$z_3 := x_3 - \alpha_1, \tag{9}$$

$$z_5 := F_h(x_5) - \alpha_3. \tag{10}$$

where x_{1d} is the desired angle of the HS and α_1 and α_3 are backstepping stabilising functions to be determined. Following the recursive backstepping procedure, the IBC for the HS is designed as follows.

Step 1:

Select a Control Lyapunov Function (CLF) candidate as:

$$V_1 = \frac{\lambda_1}{2}{\chi_1}^2 + \frac{1}{2}{z_1}^2. \tag{11}$$

Table 1
Physical parameters of the TRAS [37].

Symbol	Description	Value
l_t	Length of the tail part of the beam	0.216 m
l_m	Length of the main part of the beam	0.202 m
k_h	Friction constant of the tail propeller subsystem	5.900×10^{-2} N m
k_v	Friction constant of the main propeller subsystem	1.271×10^{-2} N m
k_{vh}	Vertical angular momentum of the tail rotor	4.200×10^{-3} N m s
k_{hv}	Horizontal angular momentum of the main rotor	-1.780×10^{-2} N m s
A	Mechanical constant	0.0652
B	Mechanical constant	0.0707
C	Mechanical constant	0.0046
D	Mechanical constant	6.4608×10^{-4}
E	Mechanical constant	0.0279
F	Mechanical constant	0.0021
I_h	Moments of inertia of the tail rotor	2.703×10^{-5} kg m^2
I_v	Moments of inertia of the main rotor	1.639×10^{-4} kg m^2
a_1	Constant	3.300×10^{-6}
a_2	Constant	9.280×10^{-6}
g	Gravitational acceleration	9.810 m s^{-2}
J_v	Sum of moments of inertia relative to the horizontal axis	3.070×10^{-2} kg m^2

where $\chi_1 = \int_0^t z_1(\tau)\, d\tau$ and λ_1 is a positive constant.

Therefore,

$$\dot{V}_1 = \lambda_1 \chi_1 \dot{\chi}_1 + z_1 \dot{z}_1 = \lambda_1 \chi_1 z_1 + z_1 (x_3 - \dot{x}_{1d}). \tag{12}$$

A stabilising function $\alpha_1(x_1)$ for z_1 is designed by taking x_3 as the virtual control.

$$\alpha_1(x_1) = -c_1 z_1 - \lambda_1 \chi_1 + \dot{x}_{1d}, \quad c_1, \lambda_1 > 0. \tag{13}$$

Hence,

$$\dot{V}_1 = -c_1 {z_1}^2. \tag{14}$$

Step 2:

Select a CLF

$$V_3 = V_1 + \frac{1}{2} {z_3}^2. \tag{15}$$

Its derivative is

$$\dot{V}_3 = \lambda_1 \chi_1 \dot{\chi}_1 + z_1 \dot{z}_1 + z_3 \dot{z}_3. \tag{16}$$

The resultant dynamics of z_1 is

$$\dot{z}_1 = z_3 - c_1 z_1 - \lambda_1 \chi_1. \tag{17}$$

With $\dot{z}_3 = \dot{x}_3 - \dot{\alpha}_1(x_1)$, the dynamics of z_3 is

$$\dot{z}_3 = \frac{1}{J_h} [l_t F_h(x_5) \cos x_2 - k_h x_3 - a_1 x_3 |x_5|] - \frac{\partial \alpha_1}{\partial x_1} \dot{x}_1. \tag{18}$$

Substituting (17) and (18) into (16), $\dot{V}_3$ is obtained as

$$\dot{V}_3 = -c_1 z_1^2 + z_3 \left[z_1 + \frac{l_t}{J_h} (F_h(x_5) \cos x_2) - \frac{1}{J_h} (k_h x_3 + a_1 x_3 |x_5|) - \frac{\partial \alpha_1}{\partial x_1} \dot{x}_1 \right]. \tag{19}$$

The stabilising function $\alpha_3(x_1, x_3)$ is designed by taking $F_h(x_5)$ as the virtual control.

$$\alpha_3 = \frac{J_h}{l_t \cos x_2} \left[-z_1 + \frac{1}{J_h} (k_h x_3 + a_1 x_3 |x_5|) + \frac{\partial \alpha_1}{\partial x_1} \dot{x}_1 - c_3 z_3 \right]. \tag{20}$$

So that,

$$\dot{V}_3 = -c_1 {z_1}^2 - c_3 {z_3}^2, \qquad c_1, c_3 > 0. \tag{21}$$

Step 3:

Finally, the full state control input u_h is designed to stabilise the entire HS.

Select a CLF as

$$V_5 = V_3 + \frac{1}{2} {z_5}^2. \tag{22}$$

Its derivative is

$$\dot{V}_5 = \lambda_1 \chi_1 z_1 + z_1 \dot{z}_1 + z_3 \dot{z}_3 + z_5 \dot{z}_5. \tag{23}$$

The resultant dynamics of z_3 is

$$\begin{aligned} \dot{z}_3 &= \dot{x}_3 - \dot{\alpha}_1(x_1), \\ &= \frac{1}{J_h} [(l_t F_h(x_5) \cos x_2) - k_h x_3 - a_1 x_3 |x_5|] \\ &\quad - \frac{l_t \cos x_2}{J_h} \alpha_3 + \frac{l_t \cos x_2}{J_h} \alpha_3 - \frac{\partial \alpha_1}{\partial x_1} \dot{x}_1. \end{aligned} \tag{24}$$

Therefore,

$$\begin{aligned} \dot{z}_3 &= \frac{l_t \cos x_2}{J_h} (F_h(x_5) - \alpha_3) - \frac{1}{J_h} (k_h x_3 + a_1 x_3 |x_5|) \\ &\quad - \frac{\partial \alpha_1}{\partial x_1} \dot{x}_1 + \frac{l_t \cos x_2}{J_h} \alpha_3. \end{aligned} \tag{25}$$

Substituting for α_3 from (20) into the last term on the right-hand side of (25) yields

$$\dot{z}_3 = \frac{l_t \cos x_2}{J_h} z_5 - z_1 - c_3 z_3. \tag{26}$$

Also as $\dot{z}_5 = \dot{F}_h(x_5) - \dot{\alpha}_3(x_1, x_3)$

$$\frac{dF_h}{dt} = \frac{dF_h}{dx_5} \cdot \frac{dx_5}{dt} = \frac{dF_h}{dx_5} \cdot \frac{1}{I_h} \left(u_h - H_h^{-1}(x_5) \right). \tag{27}$$

The dynamics of $\dot{z}_5$ can be expressed as

$$\dot{z}_5 = \frac{dF_h}{dx_5} \cdot \frac{1}{I_h} \left(u_h - H_h^{-1}(x_5) \right) - \dot{\alpha}_3(x_1, x_3). \tag{28}$$

The state x_5 is available and when measured directly, $I_h = 1$ and (28) can then be expressed as:

$$\dot{z}_5 = \frac{dF_h}{dx_5} \left(u_h - H_h^{-1}(x_5) \right) - \frac{\partial \alpha_3}{\partial x_1} \dot{x}_1 - \frac{\partial \alpha_3}{\partial x_3} \dot{x}_3. \tag{29}$$

Substituting (17), (26) and (28) into (23) yields

$$\dot{V}_5 = -c_1 z_1^2 - c_3 z_3^2 + z_5 \left[\frac{l_t \cos x_2}{J_h} z_3 + \frac{dF_h}{dx_5} \left(u_h - H_h^{-1}(x_5) \right) - \frac{\partial \alpha_3}{\partial x_1} \dot{x}_1 - \frac{\partial \alpha_3}{\partial x_3} \dot{x}_3 \right]. \tag{30}$$

To stabilise the dynamics of z_5, the control input u_h is designed as:

$$u_h = H_h^{-1}(x_5) + \frac{1}{\frac{dF_h}{dx_5}}\left(-\frac{l_t \cos x_2}{J_h} z_3 + \frac{\partial \alpha_3}{\partial x_1}\dot{x}_1 + \frac{\partial \alpha_3}{\partial x_3}\dot{x}_3 - c_5 z_5\right). \tag{31}$$

So that,

$$\dot{V}_5 = -c_1 z_1^2 - c_3 z_3^2 - c_5 z_5^2 \leq 0, \qquad c_1, c_3, c_5 > 0. \tag{32}$$

Analytically evaluating the partial derivatives and substituting for z_3 and z_5 in (31) yields the control law for the HS

$$\begin{aligned} u_h = {} & H_h^{-1}(x_5) + \frac{1}{\frac{dF_h}{dx_5}}\left\{-\frac{l_t \cos x_2}{J_h}(x_3 + c_1 z_1 + \lambda_1 \chi_1 - \dot{x}_{1d})\right. \\ & - \frac{J_h}{l_t \cos x_2} x_3 [1 + \lambda_1 x_3 \\ & + c_3 (c_1 + \lambda_1 z_1)] \\ & + \frac{J_h}{l_t \cos x_2}\dot{x}_3 \left[\frac{1}{J_h}(k_h + a_1 |x_5|) - c_1 - c_3 - \lambda_1 z_1\right] \\ & \left. - c_5 [F_h(x_5) - \alpha_3 (x_1, x_1)]\right\}. \end{aligned} \tag{33}$$

3.2. Vertical subsystem integral backstepping

The decomposed model for the VS of the TRAS is obtained as [37]

$$\begin{aligned} \dot{x}_2 &= x_4 \\ \dot{x}_4 &= \frac{1}{J_v}[l_m F_v(x_6) - k_v x_4 + g((A - B)\cos x_2 - C \sin x_2) \\ &\quad - a_2 x_4 |x_6|] \\ \dot{x}_6 &= \frac{1}{I_v}\left(u_v - H_v^{-1}(x_6)\right). \end{aligned} \tag{34}$$

Let:

$$z_2 := x_2 - x_{2d}, \tag{35}$$

$$z_4 := x_4 - \alpha_2, \tag{36}$$

$$z_6 := F_v(x_6) - \alpha_4. \tag{37}$$

where x_{2d} is the desired pitch angle and α_2 and α_4 are stabilising functions to be obtained in the backstepping design. Using a similar design approach for the HS, the control laws for the VS are obtained as

$$\alpha_2(x_2) = -c_2 z_2 - \lambda_2 \chi_2 + \dot{x}_{2d}, \quad c_2, \lambda_2 > 0 \tag{38}$$

where $\chi_2 = \int_0^t z_2(\tau)\, d\tau$ and λ_2 is a positive constant, and

$$\begin{aligned} \alpha_4 = {} & \frac{J_v}{l_m}\left(-z_2 + \frac{1}{J_v}(G(x_2) + k_v x_4 + a_2 x_4 |x_6|)\right. \\ & \left. + \frac{\partial \alpha_2}{\partial x_2}\dot{x}_2 - c_4 z_4\right). \end{aligned} \tag{39}$$

where $G(x_2) = -g((A - B)\cos x_2 - C \sin x_2)$ is the return moment of the VS.

Such that,

$$\dot{V}_4 = -c_2 {z_2}^2 - c_4 {z_4}^2, \quad c_2, c_4 > 0 \tag{40}$$

and

$$u_v = H_v^{-1}(x_6) + \frac{1}{\frac{dF_v}{dx_6}}\left(-\frac{l_m}{J_v} z_4 + \frac{\partial \alpha_4}{\partial x_2}\dot{x}_2 + \frac{\partial \alpha_4}{\partial x_4}\dot{x}_4 - c_6 z_6\right). \tag{41}$$

Such that,

$$\dot{V}_6 = -c_2 {z_2}^2 - c_4 {z_4}^2 - c_6 {z_6}^2, \qquad c_2, c_4, c_6 > 0. \tag{42}$$

The final control law for the VS is obtained by evaluating the partial derivatives and substituting for z_4 and z_6 in (41)

$$\begin{aligned} u_v = {} & H_v^{-1}(x_6) + \frac{1}{\frac{dF_v}{dx_6}}\left\{-\frac{l_m}{J_v}(x_4 + c_2 z_2 + \lambda_2 \chi_2 - \dot{x}_{2d})\right. \\ & - \frac{J_v}{l_m} x_4 \left[1 - \frac{1}{J_v}\dot{G}(x_2)\right. \\ & \left. + \lambda_2 x_4 + c_4 (c_2 + \lambda_2 z_2)\right] \\ & + \frac{J_v}{l_m}\dot{x}_4 \left[\frac{1}{J_v}(k_v + a_2 |x_6|) - c_2 - c_4 - \lambda_2 z_2\right] \\ & \left. - c_6 [F_v(x_6) - \alpha_4 (x_2, x_4)]\right\}. \end{aligned} \tag{43}$$

4. Improvement of the transient response and reference tracking

In this section, the modified method of dual boundary conditional integration for transient performance improvement and technique of tracking improvement based on switching and control signal saturation for the HS and VS respectively are presented.

4.1. Modified dual boundary conditional integral (MDBCI) gain law

Consider a closed-loop system with a bounded reference $r(t)$, output $y(t)$ controlled by a continuous signal $u(t)$ augmented by a saturated integrator χ with integral gain $\lambda(t)$ to eliminate steady state error. Let the error in the system be defined as a compact set $z(t) = y(t) - r(t)$. Assuming $|z(0)| > 0$, let μ and δ $(|z(0)| > \mu > \delta > 0)$ respectively, be the widths of outer and inner boundary layers containing $r(t)$. The integral gain law (44) is proposed to provide variable integral action to robustify the system without degrading the transient performance and illustrated in Fig. 2.

$$\lambda(t) = \begin{cases} 0, & |z| > \mu > \delta \\ \lambda_r, & \mu \geq |z| > \delta \\ \lambda_r + \int (\operatorname{sgn}(z(t)).k_\lambda |z(t)| + k_r |\dot{x}_d|)dt, & |z| \leq \delta, t < t_{ss} \\ \lambda_r + \int (k_\lambda |z(t)| + k_r |\dot{x}_d|)dt, & |z| \leq \delta, t \geq t_{ss}. \end{cases} \tag{44}$$

For $0 \leq \lambda_r < \lambda_m$ where $\lambda_m \epsilon \mathbb{R}^+$ is the minimum integral gain required to achieve adequate tracking, $\lambda_r < \lambda_m$ is the integral gain within the outer boundary layer, k_λ and k_r are positive tuning constants and t_{ss} is a predetermined time instant after the transient period beyond which $\lambda(t)$ cannot decrease in value.

Remark 2. Let $y_{\lambda_o}(t)$ be the output of the system with no integral action in the neighbourhood of $r(t)$ and $y_{\lambda_m}(t)$ be the output with sufficient integral action which adequately tracks $r(t)$ after the transient period. The bifurcation point y_b which is contained within μ is defined as the value of $y_{\lambda_o}(t)$ during the transient period where the output with sufficient integral action diverges from the output with no integral action i.e. $y_b := \max |y_{\lambda_o}| \Big|_{|y_{\lambda_m} - y_{\lambda_o}| \geq \varepsilon}$, where ε is a small positive constant.

Remark 3. For constant waveforms, t_{ss} is any time instant after the output has settled to within 2% of the reference value. For sinusoidal references, however, t_{ss} is a predetermined peak instant of the reference signal.

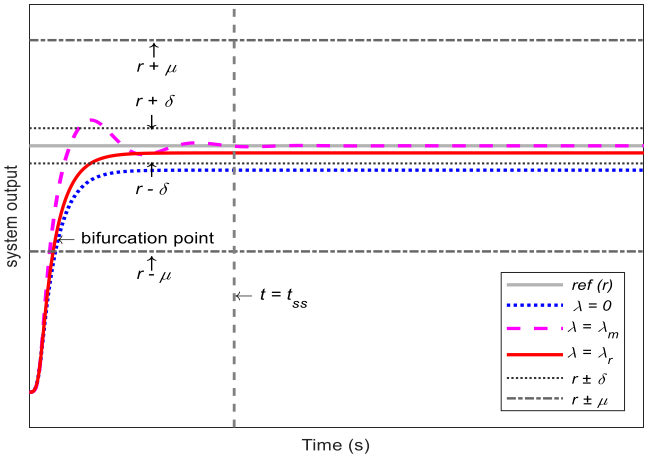

Fig. 2. Tuning of λ_m, λ_r, width of the outer boundary μ and width of the inner boundary, δ..

Remark 4. The integral gain law in (44) improves the result of [17] in such a way that mechanism in (44) automatically addresses both constant and time varying reference signals owing to the $k_r\,|\dot{x}_d|$ term. Also, the sign of the incremental gain during the transient phase in (44) depends on the sign of the error state and not on the derivatives of the reference input as in [17].

4.2. Tracking improvement of the TRAS

As mentioned earlier, the HS is an undamped system with a low friction coefficient driven by a bi-directional motor in order to permit rotation in the yaw axis in opposite directions. This makes the HS very sensitive to the actuator output. A switched control framework between two candidate backstepping control laws realised at different steps of the recursive backstepping procedure is used to maintain good asymptotic reaching behaviour and tracking performance. The control law in (33) is a full state controller for the relative degree 3 system and serves as the first candidate controller and gives true asymptotic convergence.

The second candidate control law is realised from the second step of the design procedure as

$$u_h = {F_h}^R(\alpha_3), \tag{45}$$

where ${F_h}^R$: $\mathbb{R} \to \mathbb{R}$ is a reverse map of the HS actuator dynamics from input to output in (3)–(4) experimentally obtained in [37]. The simplified control law (45) is independent of the noisy acceleration $\dot{x}_3$ of the beam and serves the purpose of tracking with less jerking. A hysteresis switching rule based on the error z_1 combined with a time delay is used to trigger controller switching from (33) to (45). The switching takes place after the transient period when z_1 enters a predetermined zone in the neighbourhood of the origin.

In the case of the VS, its natural damping and saturation i.e. limiting the control signal are used to reduce the jerking effects in the main rotor. The counterbalance weights of the TRAS are adjusted to provide damping such that the main part of the beam is lowered about −0.5 rad from the horizontal. The control actuation signal is then limited to $-\gamma \leq u_v \leq 1$ where γ is a small positive constant. This allows the main rotor to produce maximum upward thrust for upward motion and allows downward motion by gravitation. Although this approach increases of the damping of the VS and its nonlinearity (by saturation), the nonlinear control design equipped with the variable integral gain law in (44) guarantees satisfactory performance.

5. Stability analysis

The stability of the TRAS under the cross coupling uncertainties with the proposed control approach is analysed in this section.

5.1. Stability of the HS

The uncertainty in the HS from (1) is given as

$$\Delta f_h = u_v k_{vh}. \tag{46}$$

The closed-loop dynamics of the HS and the uncertainty in (46) can be expressed in matrix form in the z coordinates from (17), (26) and (29) as

$$\dot{z}_h = \begin{bmatrix} -c_1 & 1 & 0 \\ -1 & -c_3 & \dfrac{l_t \cos x_2}{J_h} \\ 0 & -\dfrac{l_t \cos x_2}{J_h} & -c_5 \end{bmatrix} z_h + \begin{bmatrix} -\lambda_1 \chi_1 \\ \Delta f_h \\ 0 \end{bmatrix} \tag{47}$$

where $z_h = \begin{bmatrix} z_1 & z_3 & z_5 \end{bmatrix}^T$.

Let

$$V_h = \frac{\lambda_1}{2}{\chi_1}^2 + \frac{1}{2}{z_h}^T z_h. \tag{48}$$

Its derivative along the dynamics of z_h is

$$\dot{V}_h = -\sum_{i=1,3,5} c_i {z_i}^2 + z_3 \Delta f_h \leq -2 \min(c_i) \frac{1}{2}{z_h}^T z_h + z_3 \Delta f_h, \tag{49}$$

or

$$\dot{V}_h \leq -\min(c_h) \|z_h\|^2 + |z_3 \Delta f_h| \tag{50}$$

where $c_h = [c_1\, c_3\, c_5]$.

Since Δf_h is bounded (u_v is bounded) it can be assumed there exists a bounded positive constant p_h such that $p_h \|z_h\|^2 \geq |z_3 \Delta f_h|$, $\forall t \geq 0$.

Theorem 1. *If* $\min(c_h) > p_h$ *then the HS of the TRMS will be asymptotically stable for the control laws* (33) *and* (45) *with* λ_1 *defined by* (44) *for the outer and inner boundary layers* μ_h *and* δ_h *respectively.*

Proof. The proof will examine the closed-loop system in the different regions of interest.

Region 1: $|z_1| > \mu_h > \delta_h$

The tracking error is exterior to the outer boundary layer and $\lambda_1 = 0$. The controller is thus reduced to a backstepping controller with no integral action. Calculating the derivative of V_h along the closed loop trajectories of the HS yields

$$\dot{V}_h \leq -\min(c_h) \|z_h\|^2 + |z_3 \Delta f_h| < 0. \tag{51}$$

Thus, the proposed control law in (33) is active and exponentially stabilising. The magnitude of the tracking error $|z_1|$ will thus decrease into region 2.

Region 2: $\mu_h \geq |z_1|$

When the tracking error lies between the two boundary layers the integral gain $\lambda_1 = \lambda_{r_h}$. Also, when $|z_1| \leq \delta_h$ (within the inner boundary) the integral gain cannot change instantaneously. The derivative of V_h along the dynamics of z_h now becomes

$$\dot{V}_h \leq -\min(c_h) \|z_h\|^2 + |z_3 \Delta f_h| \leq 0 \tag{52}$$

which is only negative semi-definite. However, all signals are bounded since $\dot{V}_h$ is non-positive and it can be deduced from Barbalat's lemma that the closed-loop system will be asymptotically stable for the proposed control input u_h in (33). That is $\lim_{t\to\infty} z_5, z_3, z_1 \to 0$.

Remark 5. After switching, $u_h = u_{h_2}, c_h = [c_1\, c_3], z_h = [z_1\, z_3]$ and the dynamics of $\dot{z}_h$ reduces to

$$\dot{z}_h = \begin{bmatrix} -c_1 & 1 \\ -1 & -c_3 \end{bmatrix} z_h + \begin{bmatrix} -\lambda_1 \chi_1 \\ \Delta f_h \end{bmatrix} \tag{53}$$

Thus V_h satisfies Branicky's non-increasing condition [41] and the system's stability is maintained for $\min(c_h) > p_h$.

5.2. Stability of the VS

The uncertainty in the VS from (1) is given as

$$\Delta f_v = -\frac{1}{2} x_3{}^2 (A + B + C) \sin(2x_2)\, u_h k_{hv} + u_h k_{hv}. \tag{54}$$

With the uncertainty (54), the closed-loop dynamics of the VS can be expressed in the z coordinates as

$$\dot{z}_v = \begin{bmatrix} -c_2 & 1 & 0 \\ -1 & -c_4 & \frac{l_m}{J_v} \\ 0 & -\frac{l_m}{J_v} & -c_6 \end{bmatrix} z_v + \begin{bmatrix} -\lambda_2 \chi_2 \\ \Delta f_v \\ 0 \end{bmatrix} \tag{55}$$

where $z_v = \begin{bmatrix} z_2 & z_4 & z_6 \end{bmatrix}^T$.

Let

$$V_v = \frac{\lambda_2}{2} \chi_2{}^2 + \frac{1}{2} z_v{}^T z_v. \tag{56}$$

Its derivative along the dynamics of z_v is

$$\dot{V}_v = -\sum_{i=2,4,6} c_i z_i{}^2 + z_4 \Delta f_v \leq -\min(c_v) \|z_v\|^2 + |z_4 \Delta f_v|, \tag{57}$$

where $c_v = [c_2\, c_4\, c_6]$.

The uncertainty $\Delta f_v(x_2, x_3, u_h)$ is bounded since u_h bounded and x_3 is in the neighbourhood of zero since the HS is stable. Alsox_2 is physically restrained between $-\pi/2 < x_2 < \pi/2$. It can be thus be assumed there exists a bounded positive constant p_v such that $p_v \|z_v\|^2 \geq |z_4 \Delta f_v|, \forall t \geq 0$.

Theorem 2. *If $\min(c_v) > p_v$, then the VS of the TRMS will be semi-globally asymptotically stable for the control law proposed in (43) and with λ_2 defined by (44) for the boundary layers μ_h and δ_h respectively.*

Proof. Similar arguments for the HS can be applied to show the semi-global asymptotic stability of the VS subjected to the physical restraint $-\pi/2 < x_2 < \pi/2$.

6. Implementation and experimental results

The modified dual boundary conditional integral switched (MDBCIS) backstepping and modified dual boundary conditional integral (MDBCI) backstepping controllers proposed for the HS and VS respectively are implemented in this section. The MDBCI(S) backstepping controllers are tested by experiment on the TRAS in real time under different operating conditions. The operating range is investigated with a step and 0.025 Hz sine wave reference similar to [42], the more rigorous 0.05 Hz sinusoidal trajectory in [32] and a square wave signal. The performance of the proposed MDBCI(S) method is also examined by comparing the responses with backstepping under (1) No integration (NOI), (2) Conventional integration (CVI) i.e. when integral action is applied at $t = 0$, (3) Conditional integration (CDI) proposed in [15] and (4) DBCI suggested in [17]. The transient response characteristics and integral absolute error (IAE) computed at a sampling time of 0.05 secs are used to assess closed-loop performance.

6.1. State estimation

Practical implementation of the IBCs requires the estimation of system states that cannot be measured directly. The Enhanced Differentiator (ED) specifically designed for systems with low speeds [43] showed better performance when compared with the Sliding Mode differentiator [44] used in [32]. In this work, the ED is thus adopted to provide estimates of the velocity of the beam $x_3(x_4)$ for the HS (VS) from only position measurements of $x_1(x_2)$. The added requirement for the acceleration of the beam $\dot{x}_3(\dot{x}_4)$ for the HS (VS) is realised by solving its corresponding expression in from measurements of $x_1(x_2)$, $x_5(x_6)$ and the estimate of $x_3(x_4)$. This eliminates the need to reuse the differentiator which results in high noise amplification. The ED for a given reference signal $r(t)$ is expressed as [43]

$$\begin{aligned} \dot{q}_1 &= q_2 \\ \dot{q}_2 &= R^2 \left[-\beta_0 (q_1 - r) - \beta_1 (q_1 - r)^{n/m} - \beta_2 \left(\frac{q_2}{R} \right)^{n/m} \right] \end{aligned} \tag{58}$$

where $q_1(t)$ and $q_2(t)$ represent the estimated states of $r(t)$ and $\dot{r}(t)$, $R, \beta_0, \beta_1, \beta_2 > 0$ and $m > n$ are positive odd numbers.

6.2. Integral gain law and ED parameters

The integral law parameters for the HS are set at $\lambda_{r_h} = 0.35, \lambda_{m_h} = 1.3, k_{\lambda_h} = 2.5, k_{r_h} = 0.5$. The widths of the outer and inner boundary regions are respectively set at $\mu_h = 0.4$ and $\delta_h = 0.075$. The HS′ ED parameters are set at $R_h = 90, \beta_{0_h} = 1, \beta_{1_h} = 1, \beta_{2_h} = 1, m_h = 201$ and $n_h = 199$. The integral gain law parameters for the VS are set at $\lambda_{r_v} = 0.85, \lambda_{m_v} = 2.0, k_{\lambda_v} = 3.0, k_{r_v} = 2.0$ with the widths of the boundary layers set at $\mu_v = 0.4$ and $\delta_v = 0.05$. The ED parameters for the VS are set at $R_v = 25, \beta_{0_v} = 2, \beta_{1_v} = 3, \beta_{2_v} = 4, m_v = 101$ and $n_v = 99$.

6.3. Step response and optimisation issues

A problem that often arises in poorly modelled processes is optimisation. When the system model is imprecise, parameters obtained via optimisation approaches may not be directly applicable to control the real plant especially when precision is desired. Fig. 3a is the fitness function value obtained via genetic algorithm optimisation on the model of TRAS using a similar reference, objective function and genetic algorithm parameters proposed for the TRMS in [42]. The best fit obtained corresponds to $c_1 = 1.46, c_2 = 1.44, c_3 = 6.40, c_4 = 5.03, c_5 = 9.32, c_6 = 9.86, \lambda_1 = 1.35$ and $\lambda_2 = 0.067$. These values were acquired with the integrator χ_1 and control signal saturated u_h at ± 0.1 and ± 0.5 respectively for the HS and integrator χ_2 saturated at ± 0.1 with the control signal u_v limited between $-\gamma$ and $+1$ for the VS with γ taken as 0.2.

While the simulation results in Fig. 3b show good transient response and tracking, application of the same values of the control parameters on the actual laboratory helicopter lead to overshoot in the HS and steady state error in the damped VS as depicted in Fig. 3c with CVI. The response with NOI i.e. setting the integral gains to zero, reduces the overshoot in the HS but decreases its tracking precision and also leads to visible steady state error in the VS. With the proposed method of MDBCI(S) however, the integral gains obtained in the optimisation process are discarded and the law in (44) is adopted. The evolution of the MDBCI(S) integral gain parameters in Fig. 3d lead to reduced overshoot in the HS and elimination of the steady state error in the VS. Table 2 gives the performance characteristics of the optimised system by experiment, where the values obtained under MDBCI(S) show

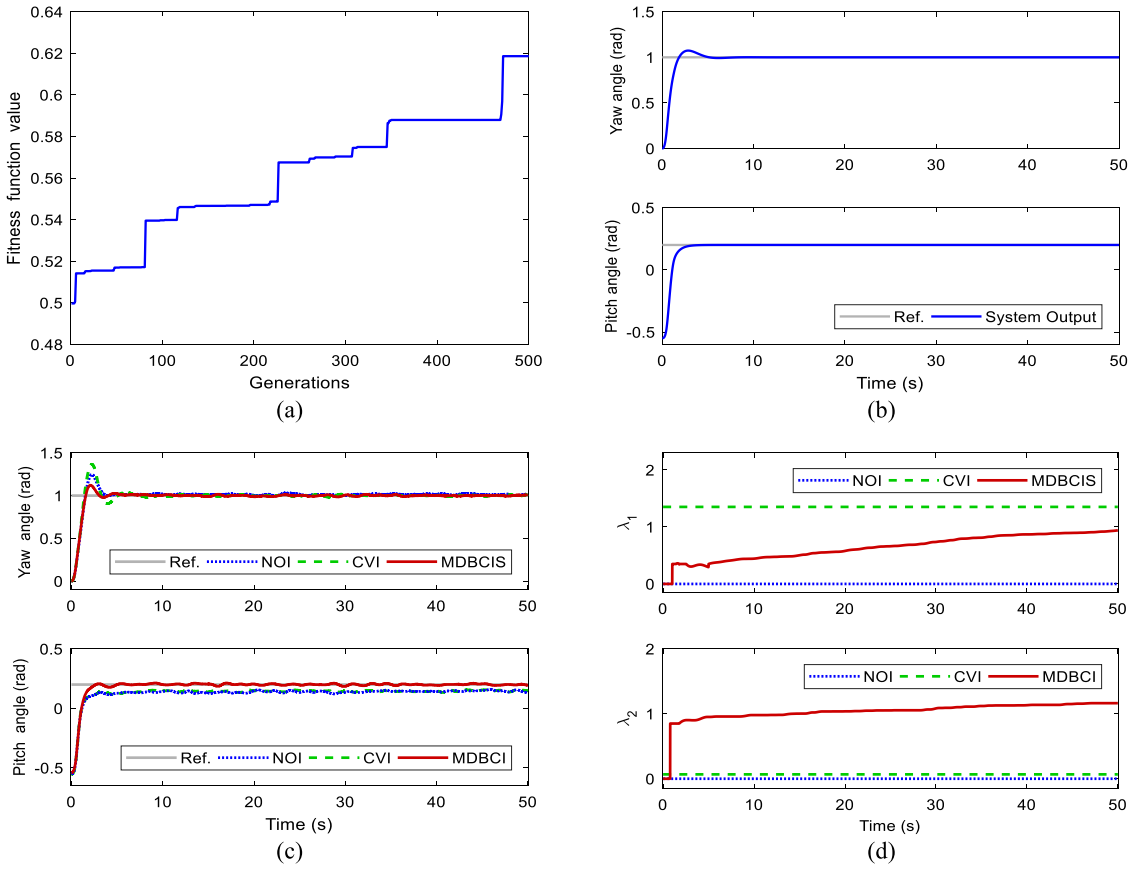

Fig. 3. Simulation and experimental results of the TRAS with optimised control parameters: (a) Fitness function, (b) Simulation angle responses, (c) Experimental angle responses, (d) Experimental integral gains.

Table 2
Optimised performance characteristics of the TRAS in 2-DOF to step inputs under no integration, conventional IBC and MDBCIS.

Performance characteristic	Axis	Control method		
		NOI	CVI	MDBCI(S)
Rise time	H	1.38	1.29	1.38
	V	2.80	2.80	1.57
Settling time	H	3.27	4.58	2.69
	V	–	–	1.98
Overshoot (%)	H	24.71	36.67	12.13
	V	0.00	0.00	2.45
IAE	H	37.42	33.53	25.70
	V	73.64	68.47	18.58

Table 3
Experimental performance characteristics of the TRAS to sinusoidal inputs under backstepping with different integration methods and MDBCI(S).

Reference		Axis	Control method			
			CVI	CDI	DBCI	MDBCI(S)
1/20 Hz	Overshoot (%)	H	34.31	9.80	5.58	7.05
		V	5.15	6.36	5.75	4.07
	IAE	H	40.78	35.92	34.43	33.77
		V	20.56	24.16	18.54	18.04
1/40 Hz	Overshoot (%)	H	20.24	18.88	12.74	9.09
		V	4.00	4.31	3.74	3.14
	IAE	H	20.22	22.22	20.18	17.40
		V	15.16	18.37	15.59	15.57

improved real time performance in comparison with CVI. For instance, the overshoot for the TRAS-HS is 12.13% with MDBCIS but rises to 36.67% with CVI. Also, the IAE for the TRAS-VS is 18.58 by MDBCI but increases to 68.47 with CVI. The much higher IAE with CVI is because the integral gain parameter obtained by optimisation of the imprecise TRAS model is too low to eliminate the steady state error in the TRAS-VS in practice and leads to results that are only slightly better than NOI.

6.4. Sine wave response

In order to allow robust tracking of a rigorous trajectory similar to [32], the control parameters are heuristically fine-tuned. The IBC parameters are retuned to $c_1 = 1.05, c_3 = 7.34$ and $c_5 = 5$ for the HS and $c_2 = 1, c_4 = 6.24$ and $c_6 = 8.0$ for the VS.

Fig. 4 shows the output responses using backstepping with CVI, CDI, DBCI and the proposed MDBCI(S) to a 0.05 Hz sinusoidal reference signal. As shown in Fig. 4, all the IBCs adequately track the trajectory for both the HS and VS. The output of the undamped HS, however, shows significant overshoot with conventional integration (CVI) as depicted in the residual error plot in Fig. 5a. The overshoot is reduced with conditional integration (CDI), DBCI and the proposed MDBCI(S) as the performance values in Table 3 indicate.

The values of the IAE in Table 3 also show that DBCI and MDBCI(S) improve precision when compared to the other methods. This is because the integral gain parameters converge to higher values ($\lambda_1 = 1.3, \lambda_2 = 2.0$) than in the cases of CVI and CDI ($\lambda_1 = 1, \lambda_2 = 1.3$) as depicted in Fig. 5b. Also, the switching method employed with MDBCIS for the undamped HS significantly reduces the jerking effects caused by measurement noise

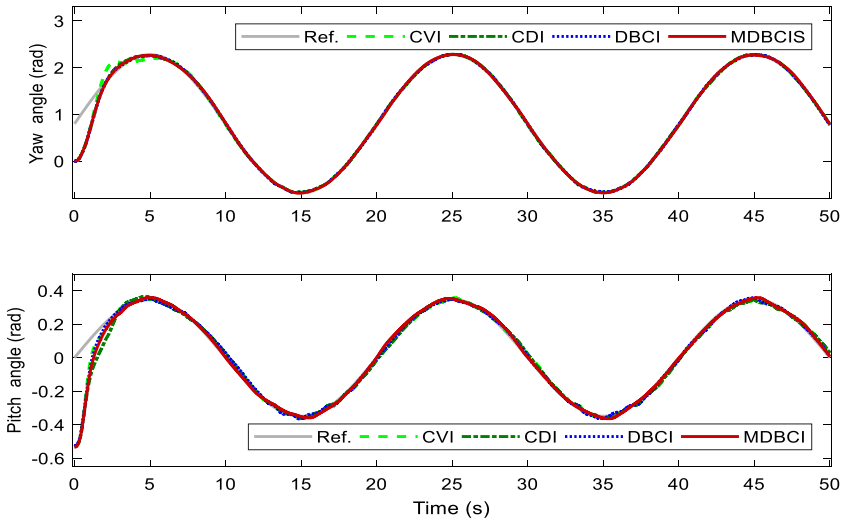

Fig. 4. Experimental cross coupled tracking responses of the TRAS to a 0.05 Hz sinusoidal signal with different integration methods and MDBCIS.

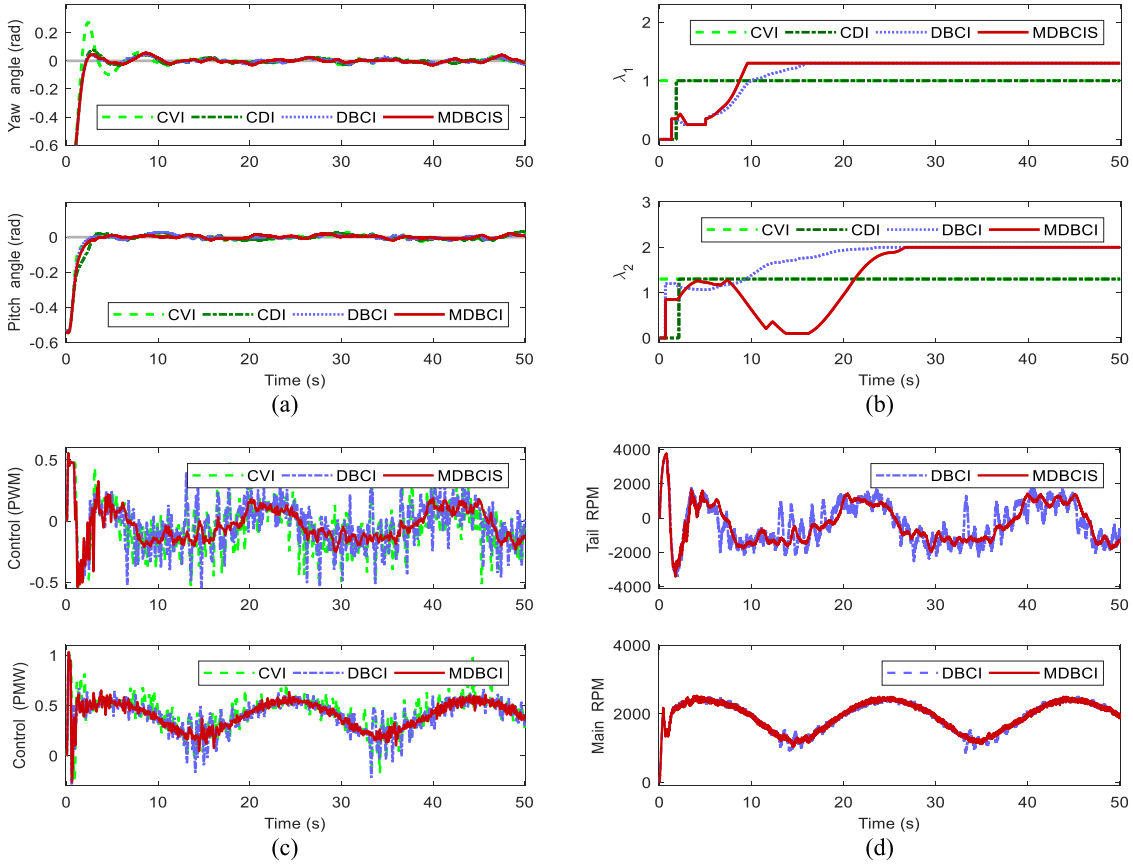

Fig. 5. Experimental cross coupled responses of the TRAS to a 0.05 Hz sinusoidal signal with different integration methods and MDBCIS: (a) Residual angle responses, (b) Integral gains, (c) Control signal (PWM), (d) Rotor speeds.

and modelling uncertainties. This can be noticed in Fig. 5c where the filtered control signal has higher peaks for DBCI (similar for CVI and CDI) as compared to MDBCIS. Although switching to mitigate measurement noise is applied only to the HS, the effects are also visible in the VS since the system is coupled.

The reduction in the jerking is better illustrated in the plot of the rotor speeds in Fig. 5d. It can be observed that in the case without switching (DBCI is plotted to illustrate this), the speed of the tail rotor has higher peaks and crosses the zero point several times (indicating a reversal in direction) in order to track the time varying reference and counter the coupling effects from the main rotor. This reversal of direction occurs less frequently with MDBCIS as Fig. 5d shows.

The adaptability of DBCI and MDBCI(S) is illustrated by reducing the amplitudes and frequencies of the reference inputs by 50% from 0.05 Hz to 0.025 Hz as shown in Fig. 6. Unlike with the previous reference, CDI now does not give any significant improvement over CVI as shown in Fig. 7a and the values in

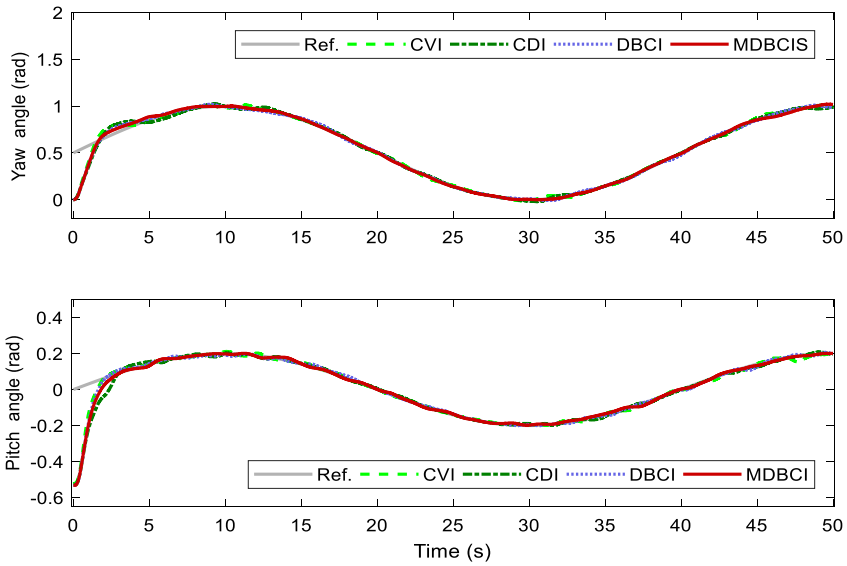

Fig. 6. Experimental cross coupled tracking responses of the TRAS to a 0.025 Hz sinusoidal signal with different integration methods and MDBCIS.

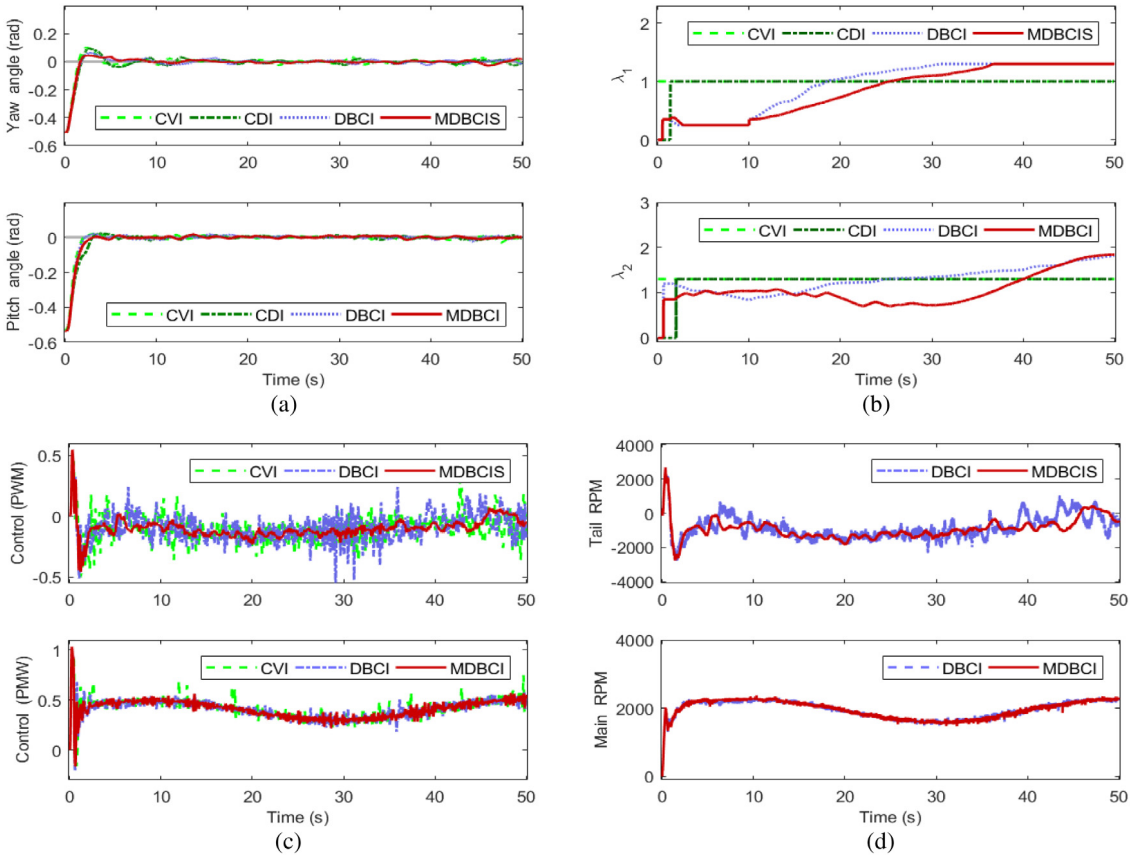

Fig. 7. Experimental cross coupled responses of the TRAS to a 0.025 Hz sinusoidal signal with different integration methods and MDBCIS: (a) Residual angle responses, (b) Integral gains, (c) Control signal (PWM), (d) Rotor speeds.

Table 3. DBCI and the proposed MDBCI(S), however, adapt to the low frequency and amplitude of the input and the integral gain parameters take longer to reach their maximum values as shown in Fig. 7b when compared to Fig. 5b. As indicated by the values in Table 3, DBCI generally leads to much improved performance when compared to CDI and CVI in terms of tracking precision and decreased overshoot which is further enhanced by MDBCI(S). Fig. 7c and Fig. 7d also show that the switching technique by the proposed MDBCIS for the HS helps to mitigate the noise and jerking of the tail rotor thereby improving energy efficiency.

6.5. Square wave response

The angle responses of the IBCs with different integration methods and MDBCI(S) to a square wave input are shown in Fig. 8. In addition to overshoots observed at every step change

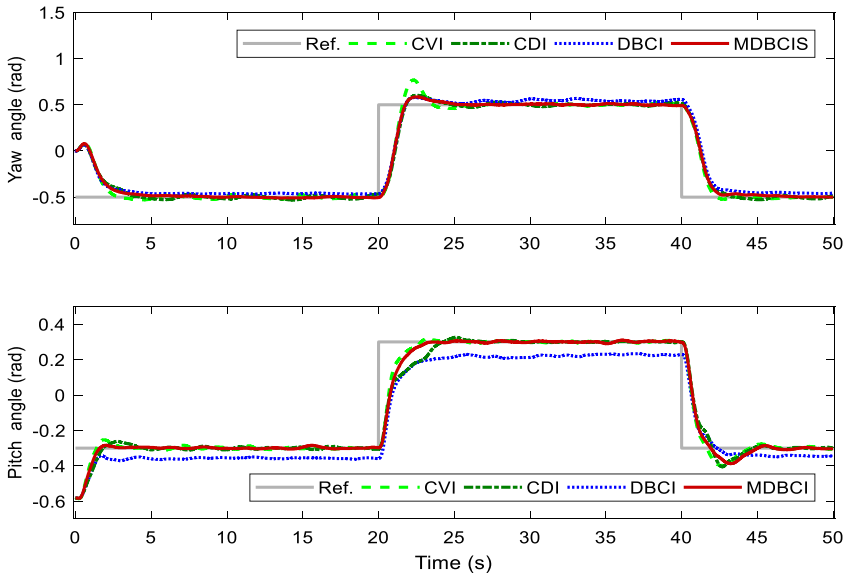

Fig. 8. Experimental cross coupled angle responses of the TRAS to a square-wave signal with different integration methods and MDBCI(S).

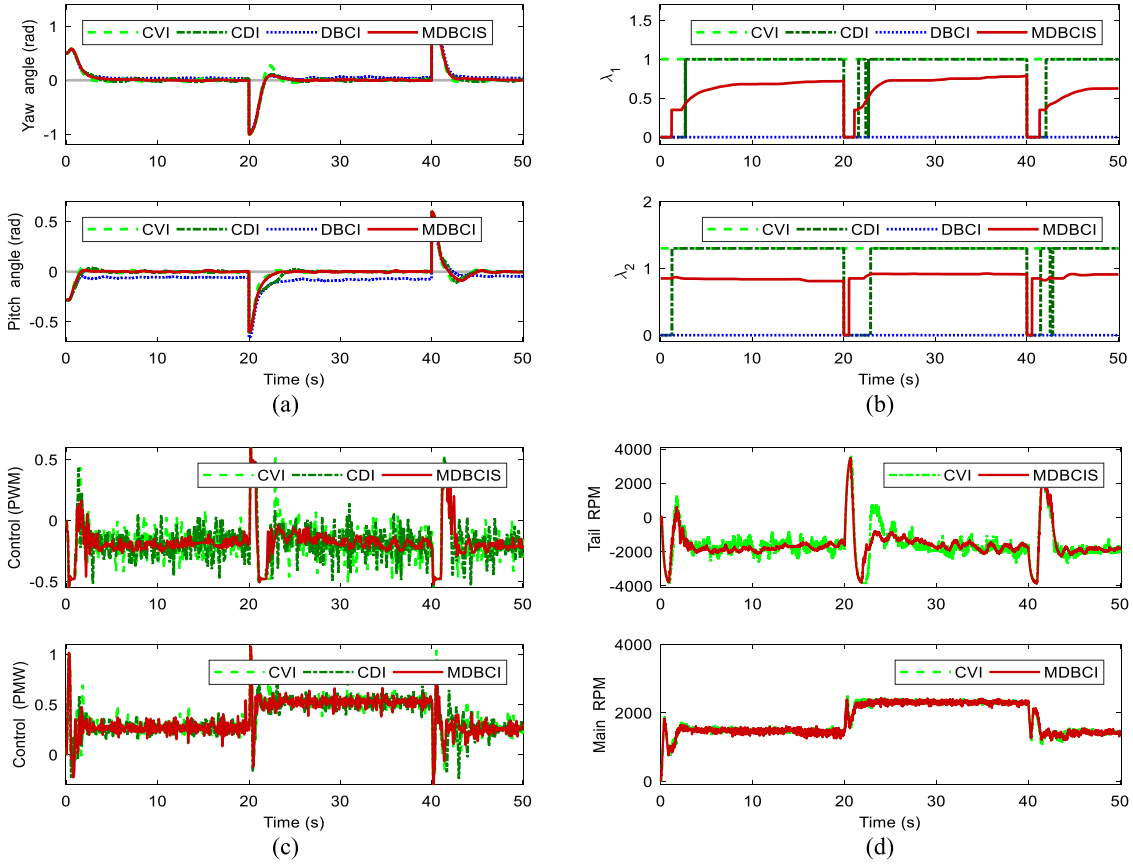

Fig. 9. Experimental cross coupled responses of the TRAS to a square wave signal with different integration methods and MDBCI(S): (a) Residual angle responses, (b) Integral gains, (c) Control signal (PWM), (d) Rotor speeds.

in the reference, a close examination of the yaw angle response in Fig. 8 and the residual plot in Fig. 9a also show persistent oscillations with CVI when the reference is low. Although the overshoots are in most cases reduced with CDI, it also exhibits oscillations in the yaw angle response at the low regions. As such, the CDI approach gives no clear improvement over CVI when the initial conditions are close to the origin. The oscillations with CVI and CDI occur mainly as a result of their integral gains being too high for the low regions of the square-wave reference signal as shown in Fig. 9b. In addition, the jerking effects from the tail rotor in Fig. 9d, as a result of the noisy control signals in Fig. 9c, lead to a further reduction in the performance of the coupled system. The response with DBCI as can be noticed in Fig. 8 is quite poor since it behaves like NOI for piecewise constant waveforms.

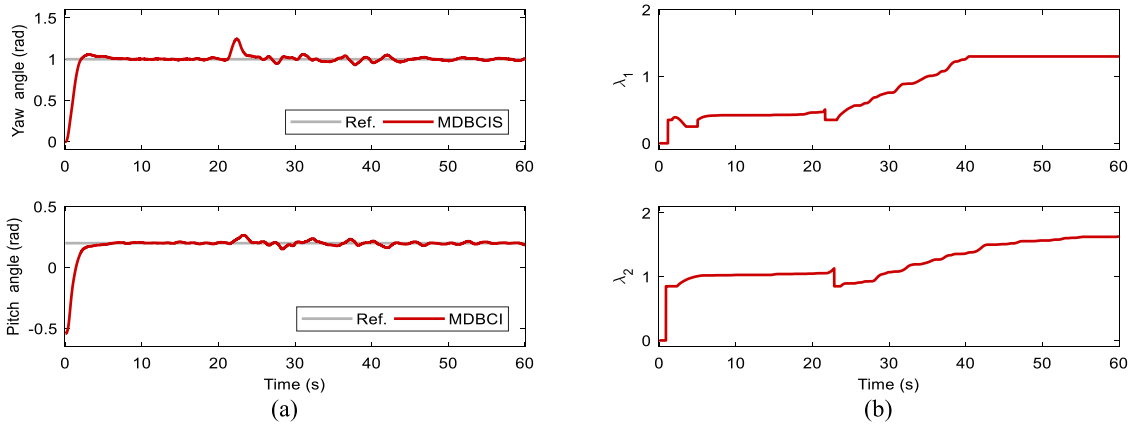

Fig. 10. Real-time robustness of the TRAS with MDBCI(S) to an external wind disturbance (a) Angular responses, (b) Integral gains.

Table 4
Experimental performance characteristics of the TRAS to a square-wave input under different integration methods and MDBCI(S).

Performance characteristic	Axis	Control method			
		CVI	CDI	DBCI	MDBCI(S)
OS_1 (%)	H	5.84	5.54	0.00	0.32
	V	16.49	13.94	0.00	5.76
OS_2 (%)	H	26.85	10.44	7.83	8.44
	V	2.41	4.46	0.00	1.13
OS_3 (%)	H	2.31	2.77	0.00	0.01
	V	16.73	17.75	6.50	14.68
IAE	H	77.49	81.15	104.47	74.89
	V	32.76	39.77	85.66	33.02

From the response in Fig. 8, it is clear that MDBCI(S) gives improved performance as the overshoots at every step change in the reference are reduced. Moreover, the yaw angle response does not exhibit the oscillatory behaviour observed with CVI and CDI. This improvement is as a result of the integral gains converging to appropriate values as shown in Fig. 9b and reduction in the control signal noise and jerking effect of the tail rotor as can be observed in Fig. 9c and 9d respectively. Although the control signals with MDBCI(S) also show some fluctuations, the deviations are comparatively smaller than in the case with CVI (and CDI) without switching. This translates into less energy consumption and a smoother response with MDBCI(S) as shown in the plot of the rotor speeds in Fig. 9d.

The overshoot and error performance characteristics of the IBCs under the different integration methods and MDBCI(S) for the square wave input are summarised in Table 4. The overshoot parameter is divided into three sections corresponding the step changes in the reference input. They are OS_1 for $0 \leq t < 20$, OS_2 for $20 \leq t < 40$ and OS_3 for $40 \leq t \leq 50$. From Table 4, the output with DBCI only exceeds the reference once for the HS and VS but is associated with steady state error owing to the lack of integral action as the IAE values show. With the exception of OS_2 for the HS where CDI has significantly reduced overshoot in comparison with CVI, the reduction in overshoot by CDI comes at the price of increased values of the IAE especially in the case of the damped VS. The performance indices, however, indicate clear improvement with MDBCI(S) as it has reduced values of all overshoots in addition to having better tracking when compared with the other methods. The only exception is in the damped VS where the IAE for CVI is slightly lower than MDBCI as a result of its faster rise time as can be observed in Fig. 8.

6.6. Robustness to external disturbances

The robustness of the proposed MDBCI(S) to an additional external disturbance is investigated by subjecting the TRAS to a wind gust from a blower aimed at the tail rotor. Fig. 10 shows how the system responds to the wind disturbance which is applied in the region between the 20 and 40 sec period. The angular responses in Fig. 10a show the visible effect of the disturbance especially in the yaw angle which reaches a peak of 1.25 rad (25% increase) in its output response. The controller, however, reacts by automatically increasing the integral gain parameter when the disturbance is activated, which helps to counter its effects. The integral gain of the HS in Fig. 10b exits the inner boundary and returns to its initial value of 0.35 before converging to the maximum. Although the disturbance is not eliminated entirely, the response shows that the system remains stable and the error returns to zero once the disturbance is deactivated. A somewhat similar response is shown by the VS which is also affected since the system is coupled. The integral gain of the VS also has a similar behaviour to that of the HS although it does not reach its allowed maximum (2.0) before the disturbance is deactivated.

Remark 6. While performance is not significantly affected by the output exiting the inner boundary, frequent exiting and re-entry can degrade performance. As such the outer boundary of the HS was increased from 0.075 to 0.1 rad (resulting in larger overshoot in the transient response) for the above robustness test to prevent this from happening. Another drawback of the MDBCI(S) approach (also shared with DBCI) is that the settling time (t_{ss}) is assumed to be known a priori.

7. Conclusion

An improved method of integral backstepping control has been designed and implemented on the helicopter-like TRAS in real time and guarantees the stability and robustness of the controlled system to uncertainties and external disturbances. The method of MDBCI(S) proposed in this paper advances the results presented in [14] in that (i) it can simultaneously and automatically handle constant and time varying reference inputs, (ii) the sign of the incremental integral gain depends only on the sign of the error signal and (iii) the performance of the coupled system is further enhanced via a switching mechanism which reduces the effects of measurement noise in the bidirectional motor of the undamped HS. The experimental results obtained showed both transient response and tracking improvement for constant and time varying reference inputs and a reduction in motor jerking

when compared with conventional, conditional and dual boundary conditional integral backstepping. Furthermore, the proposed MDBCI(S) also achieved enhanced real time performance when compared to CVI with over 24% and 23% reduction in overshoot and tracking error respectively for the HS when the control parameters were obtained via optimisation of an imprecise model of the controlled system. An area of possible future work will be to investigate the extent to which employment of a disturbance observer can further improve robustness and guarantee output regulation in the presence of the wind disturbance. It will also be interesting to investigate how the assumption regarding a priori knowledge of the settling time with MDBCI could be relaxed.

Declaration of competing interest

The authors declare that they have no known competing financial interests or personal relationships that could have appeared to influence the work reported in this paper.

References

[1] Isidori A, Byrnes CI. Output regulation of nonlinear systems. IEEE Trans Automat Control 1990;35:131–40.
[2] Astolfi D, Praly L. Integral Action in Output Feedback for multi-input multi-output nonlinear systems. IEEE Trans Automat Control 2015;62:1559–70.
[3] Skjetne R, Fossen TI. On integral control in backstepping: analysis of different techniques. In: Proceedings of the American control conference. 2004, p. 1899–904.
[4] Sheng D, Wei Y, Cheng S, Shuai J. Adaptive backstepping control for fractional order systems with input saturation. J Franklin Inst B 2017;354:2245–68.
[5] Narendra KS, Balakrishnan J. Improving transient response of adaptive control systems using multiple models and switching. IEEE Trans Automat Control 1994;39:1861–6.
[6] Kalkkuhl J, Johansen TA, Ludemann J. Improved transient performance of nonlinear adaptive backstepping using estimator resetting based on multiple models. IEEE Trans Automat Control 2002;47:136–40.
[7] Bechlioulis CP, Rovithakis GA. Adaptive control with guaranteed transient and steady state tracking error bounds for strict feedback systems. Automatica 2009;45:532–8.
[8] Davanipour M, Khayatian AR, Dehghani M, Arefi MM. A solution for enhancement of transient performance in nonlinear adaptive control: Optimal adaptive reset based on barrier Lyapunov function. ISA Trans 2018;80:169–75.
[9] Kanellakopoulos I, Krein PT. Integral-action nonlinear control of induction motors. In: Proceedings of the 12th IFAC world congress. 1993, p. 251–4.
[10] Clegg JC. A nonlinear integrator for servomechanisms. Trans Amer Inst Electr Eng II Appl Ind 1958;77:41–2.
[11] Bakkeheim J, Johansen TA, Smogeli ØN, Sorensen AJ. Lyapunov-based integrator resetting with application to marine thruster control. IEEE Trans Control Syst Technol 2008;16:908–17.
[12] Zaccarian L, Nešić D, Teel AR. Analytical and numerical Lyapunov functions for SISO linear control systems with first-order reset elements. Internat J Robust Nonlinear Control 2011;21:1134–58.
[13] Hunnekens BGB, Wouw Nvd, Nijmeijer H. Variable gain motion control for transient performance improvement. In: Proceedings of the American control conference (ACC). 2012, p. 2467–72.
[14] Hunnekens B, Wouw Nvd, Heertjes M, Nijmeijer H. Synthesis of variable gain integral controllers for linear motion systems. IEEE Trans Control Syst Technol 2015;23:139–49.
[15] Seshagiri S, Khalil HK. Robust output feedback regulation of minimum-phase nonlinear systems using conditional integrators. Automatica 2005;41:43–54.
[16] Singh A, Khalil HK. Regulation of nonlinear systems using conditional integrators. Internat J Robust Nonlinear Control 2005;15:339–62.
[17] Haruna A, Mohamed Z, Efe MÖ, Basri MAM. Dual boundary conditional integral backstepping control of a twin rotor MIMO system. J Franklin Inst B 2017;354:6831–54.
[18] Ho-Seop J, Chong-Won L. Time delay control with state feedback for azimuth motion of the frictionless positioning device. IEEE/ASME Trans Mechatronics 1997;2:161–8.
[19] Ball AA, Khalil HK. High-gain-observer tracking performance in the presence of measurement noise. In: Proceedings of the American control conference (ACC). 2009, p. 4626–7.
[20] Tilli A, Montanari M. A low-noise estimator of angular speed and acceleration from shaft encoder measurement. Automatika-Zagreb 2001;42:169–76.
[21] Wen P, Lu TW. Decoupling control of a twin rotor mimo system using robust deadbeat control technique. IET Control Theory Appl 2008;2:999–1007.
[22] Chi-Ming C, Jih-Gau J. Real time TRMS control using FPGA and hybrid PID controller. In: Proceedings of the 11th IEEE international conference on control and automation (ICCA). 2014, p. 983–8.
[23] Madoński R, Herman P. An experimental verification of ADRC robustness on a cross-coupled aerodynamical system. In: Proceedings of the IEEE international symposium on industrial electronics (ISIE). 2014, p. 859–63.
[24] Yang X, Cui J, Lao D, Li D, Chen J. Input shaping enhanced active disturbance rejection control for a twin rotor multi-input multi-output system (TRMS). ISA Trans 2016;62:287–98.
[25] Belmonte LM, Morales R, Fernández-Caballero A, Somolinos JA. A tandem active disturbance rejection control for a laboratory helicopter with variable-speed rotors. IEEE Trans Ind Electron 2016;63:6395–406.
[26] Ates A, Yeroglu C. Online tuning of two degrees of freedom fractional order control loops. Balkan J Electr Comput Eng 2016;1:5–11.
[27] Mustafa G, Iqbal N. Controller design for a twin rotor helicopter model via exact state feedback linearisation. In: Proceedings of the 8th international multitopic conference (INMIC). 2004, p. 706–11.
[28] Pandey VK, Kar I, Mahanta C. Controller design for a class of nonlinear MIMO coupled system using multiple models and second level adaptation. ISA Trans 2017;69:256–72.
[29] Su J, Liang C, Chen H. Robust control of a class of nonlinear systems and its application to a twin rotor MIMO system. In: Proceedings of the IEEE international conference on industrial technology. 2002, p. 1272–7.
[30] Saroj DK, Kar I, Pandey VK. Sliding mode controller design for twin rotor MIMO system with a nonlinear state observer. In: Proceedings of the international multi-conference on automation, computing, communication, control and compressed sensing (IMac4s). 2013, p. 668–73.
[31] Butt SS, Aschemann H. Multi-variable integral sliding mode control of a two degrees of freedom helicopter. In: Proceedings of the 8th vienna international IFAC conference on mathematical modelling (MATHMOD). 2015, p. 802–7.
[32] Rashad R, El-Badawy A, Aboudonia A. Sliding mode disturbance observer-based control of a twin rotor MIMO system. ISA Trans 2017;69:166–74.
[33] Zeghlache S, Amardjia N. Real time implementation of non linear observer-based fuzzy sliding mode controller for a twin rotor multi-input multi-output system (TRMS). Optik 2018;156:391–407.
[34] Precup RE, Radac MB, Roman RC, Petriu EM. Model-free sliding mode control of nonlinear systems: Algorithms and experiments. Inform Sci 2017;381:391–407.
[35] Pratap B, Purwar S. Real-time implementation of neuro adaptive observer-based robust backstepping controller for twin rotor control system. J Control Autom Electr Syst 2014;25:137–50.
[36] Rashad R, Aboudonia A, El-Badawy A. A novel disturbance observer-based backstepping controller with command filtered compensation for a MIMO system. J Franklin Inst B 2016;353:4039–61.
[37] Inteco corporation, two rotor aerodynamical system user manual. Available at http://www.inteco.com.pl, Krakow, Poland; 2013.
[38] Krstic M, Kanellakopoulos I, Kokotovic PV. Nonlinear and adaptive control design. New York: Wiley; 1995.
[39] Ding Z. Nonlinear and adaptive control systems. London: Institution of Engineering and Technology; 2013.
[40] Yaolong T, Jie C, Hualin T, Jun H. Integral backstepping control and experimental implementation for motion system. In: Proceedings of the IEEE international conference on control applications. 2000, p. 367–72.
[41] Branicky MS. Multiple Lyapunov functions and other analysis tools for switched and hybrid systems. IEEE Trans Automat Control 1998;43:475–82.
[42] Juang JG, Huang MT, Liu WK. PID control using presearched genetic algorithms for a MIMO system. IEEE Trans Syst Man Cybern C 2008;38:716–27.
[43] Su YX, Zheng CH, Müller PC, Duan BY. A simple improved velocity estimation for low-speed regions based on position measurements only. IEEE Trans Control Syst Technol 2006;14:937–42.
[44] Levant A. Robust exact differentiation via sliding mode technique. Automatica 1998;34:379–84.